End of study internship

Year: 2021/2022

MODELISATION AND MANUFACTURING OF A WIRELINE CABLE WITH CARBON REINFORCEMENTS

Author: Badreddine BARKI

Promotion: 2022

Academic supervisor: François AUSLENDER

Schlumberger supervisors:
François CHEVILLIARD

Internship from 14/03/2022 to 14/09/2022
Defence day: 01/09/2022

SCHLUMBERGER VECTOR S.A.S
Adress: 8 Route de Vauchelles, 80100 Abbeville Cedex

Contents

List of Figures

List of Tables

Chapter 1

Carbon / Epoxy cable

1.1 Introduction

Wireline is a type of cable used to measure physical quantities downhole in oil wells. It is usually made of copper or steel and can be used to measure pressure, temperature, and other properties. It can be in the form of a wire, metal tube or fiber optic cable. In this project, the company is looking for a new type of wireline cable made of composite materials, specifically Carbon/Epoxy.

1.2 General description

The cables consist of a centrally positioned conductor, two layers of strands (Toron) with a number and laying angle that may vary depending on the model, and an outer jacket. The number of strands and the laying angle can vary depending on the architecture and the outer jacket. In addition, each (Toron) of the composite strands is embedded in an ETFE coating.

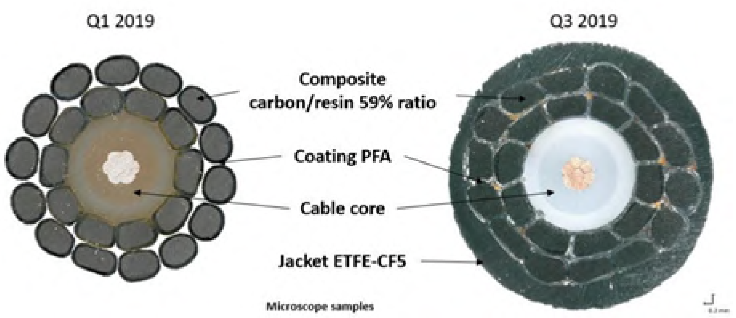

Figure 1.1: Description of the developement status of the prototype cable.

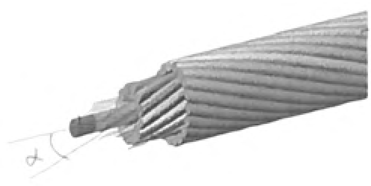

Figure 1.2: Standard composition of the cable.

Such a cable must meet the following specificities: mechanical resistance, chemical resistance, gas barrier (Gas Block), inter-strand lubrication, weldability and ideally repairability.

1.3 Material properties

Material properties evaluated (must be validated by material tests)		Jonc *HR_CF T700S Vf=58.8% Résine*	Toron=Jonc+coating		Coating *ETFE*	Gaine Extérieure *ETFE + carbone 5%*	Conducteur *PFA/CUIVRE*
		Théorique	Théorique	Essai	Fiche technique	Fiche technique	Fiche technique
Général							
Temperature		23°C	23°C	23°C	23°C	23°C	23°C
Density	*d*	1,5	-	-	1,7	1,74	2,15
Stiffness							
Axial Young modulus	*E1 (MPa)*	138000	108508	108000			
Transverse Young modulus	*E2 (MPa)*	7000		-	890	2275	590
Out of plan Young modulus	*E3 (MPa)*	7000		-			
Poisson ratio 12	*v12*	0,3		-			
Poisson ratio 13	*v13*	0,3		-	0,3	0,3	0,3
Poisson ratio 23	*v23*	0,4		-			
Shear modulus 12	*G12 (MPa)*	2500		-			
Shear modulus 13	*G13 (MPa)*	2500		-	342	875	227
Shear modulust 23	*G23 (MPa)*	2500		-			
Strength							
Axial Tensile strength	*Xt (MPa)*	2842	2265	2334	-	30	25
Axial Compression strength	*Xc (MPa)*	1000		-	-	-	-
Transverse Tensile strength	*Yt (MPa)*	40		-	-	-	-
Transverse Compression strength	*Yc (MPa)*	100		-	-	-	-
Out of plan Tensile strength	*Zt (MPa)*	40		-	-	-	-
Out of plan Compression strength	*Zc (MPa)*	100		-	-	-	-
Shear strength 12	*Sxy (MPa)*	x		-	-	-	-
Shear strength 13	*Sxz (MPa)*	x		-	-	-	-
Shear strength 23	*Syz (MPa)*	x		-	-	-	-

Table 1.1: Material Properties of the different components.

The table above demonstrate the numerous mechanical characteristics of the main components used to manufacture the cable, for every part, it defines the stiffness characteristics like Young modulus that describes the deformation behavior and Poisson coefficient that intervene mainly in the retraction of the structure, the table also defines strength values of the different components, this data is necessary for building the numerical model of the cable.

1.4 Cable manufacturing

1.4.1 Fiber manufacturing

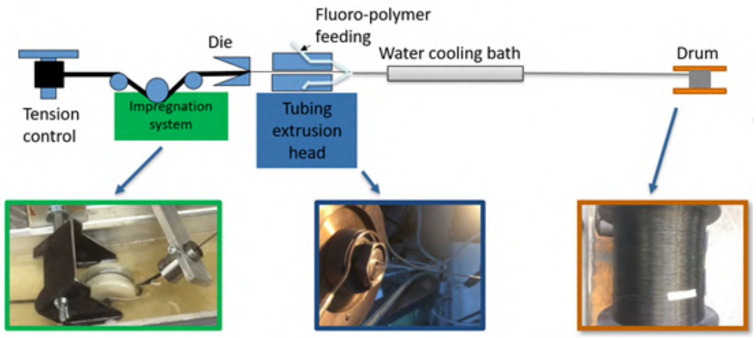

Figure 1.3: Fiber manufacturing.

The pilot line (Rosendahl) consists of 5 zones: fiber feeding, impregnation in the tank, ETFE extrusion, the pulling unit and the unit and the winder. The manufacture of the jonc is then part of a more complete industrial scheme allowing to arrive at the finished cable. This process is described in the following figure.

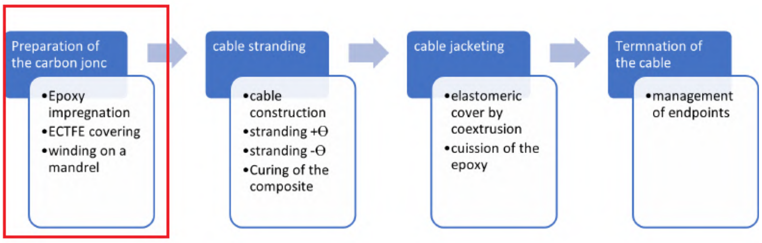

Figure 1.4: Manufacturing process of the composite reinforcement cable (Fiber manufacturing phase).

1.4.2 Cable Assembly

This step consists mainly of making an assembly to armor the conductor, and this is done by making 2 layers of carbon fiber following a configuration, that contains the number of fibers used in every layer and a lay angle for every layer also.

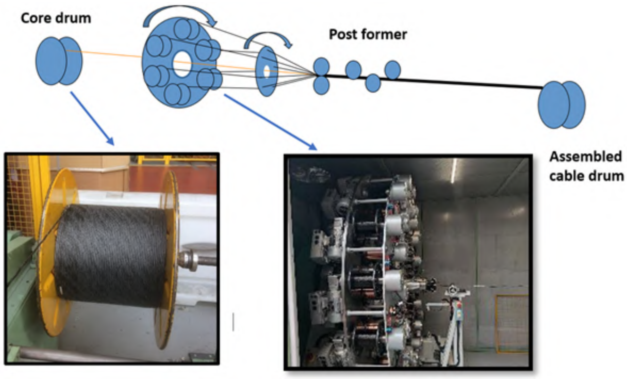

Figure 1.5: Cable assembly manufacturing.

After the preparation of the drums, they will be mounted in OMA machine to start the stranding operations, the first layer stranding takes a direction of $+\mathbf{T}$ while the second layer of armoring takes the opposite direction **-T**, after the assembly of the layers the cable go straight to curing.

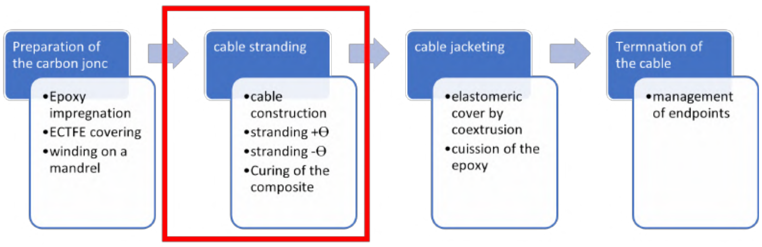

Figure 1.6: Manufacturing process of the composite reinforcement cable (Assembly phase).

The curing phase takes approximately 237 hours passing from cable aging, pre-curing, and then the curing and to make the last step is made to cable Gas block during the downhole applications and it lasts approximately 35 hours.

1.4.3 Cable jacketing

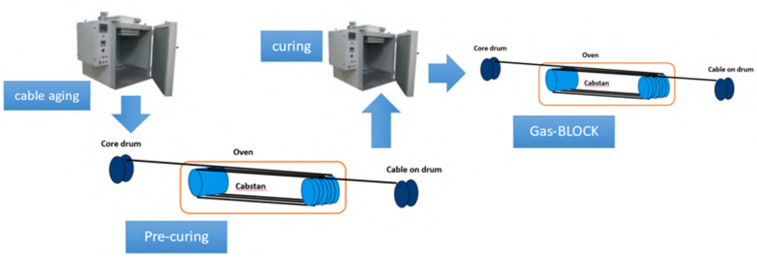

Figure 1.7: Curing of the composite.

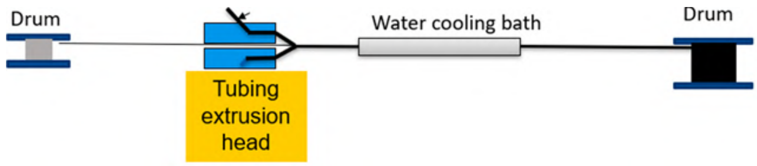

Figure 1.8: Cable jacketing process.

This is the last step of cable manufacturing, and it consists of making a coating or a jacket composed of ETFE and 5% of carbon, mainly and elastomeric cover using coextrusion.

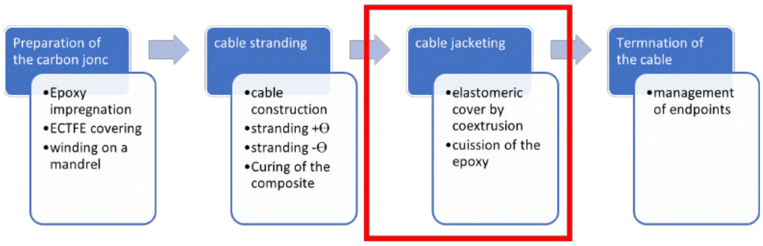

Figure 1.9: Manufacturing process of the composite reinforcement cable (Jacketing phase).

1.5 Context and objectives

The engineering team at Schlumberger wants to proceed in the building of a numerical model of the cable as well as the realization of mechanical tests on it. The challenge is to advance in the development program of the cable and thus to progress in the understanding of all the mechanisms involved in the cable's resistance.

So, based on previous models done by Cetim - the French Technical Center for Mechanical Industries we took the initiative to use the same approach used by them and follow the same step to building our own numerical model of the cable.

The model that was set to be build contains a total of 20 carbon fibers, 11 in the first layer and 9 at the second layer, this configuration was chosen based on numerous tests and research, and already 3 prototypes were made and will be used later for verification of the numerical model.

The purpose of this model is to calculate and see the behavior of the cable while changing the lay angle of the layers, and thus finding the optimum lay angles that can enhance the functioning of the cable.

1.6 Conclusion

Understanding the components and the architecture of the cable along with its manufacturing process will allow us to advance quickly in the task of the creation of the numerical model and gives us a perspective on the main parameters that can alter the performance of the cable and work to optimize them as much as possible.

Chapter 2

The numerical model of the cable

2.1 Introduction

Building the numerical model will allow us to make the changes that we think are better suited to alter the cable characteristics, and running the calculations required to enhance the cable performance and reliability.

2.2 Designing and modeling of the cable

The development of 3D helical generators with volume partition is not possible with the finite element software Abaqus due to its limited geometric creation capabilities. Therefore, it is not possible to use a fully parametrizable model in this research.

However, to create all the components that make up the cable's pieces—strands with rope portions and coatings, conductors, and sheaths—we used the CAD software Creo. For each level, only one thread is drawn. As a result, the duplication is then quickly completed in the Abaqus assembly section by means of rotating repetition, eliminating the need to enter all the strands' worth of data (mesh, material reference, definition of sets, surfaces, and sections, etc.).

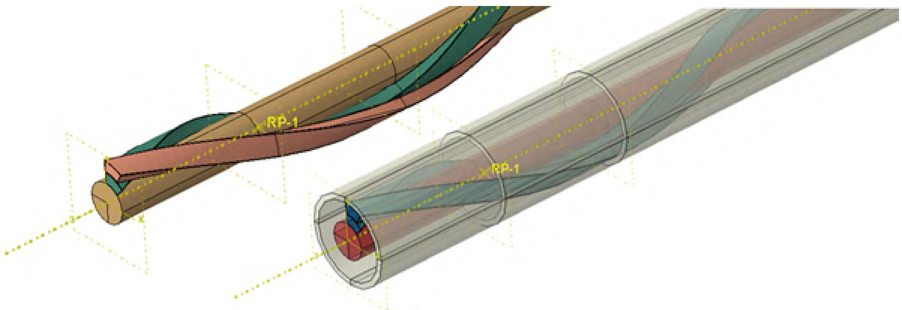

Figure 2.1: CAO model under Creo software for 11/9 configuration cabke.

In the purpose of the study and to reduce the time of simulation, a portion of 10 mm will be modelized.

We have tried to automatize the process of creating the model as we are going to need a new model with different lay angle every time, it usually takes a dozen of minutes to change all the angles and the measures associated in the sketches manually, so the idea of automatizing the process has popped out and was conducted.

By creating an excel file contains all the sketch measures needed for the creation of the cable parts, we were able to link the excel file directly to our model sketch, so by doing that we only need now to go to the file modify the measures we want and in a second the new parts will be generated, this has allowed us to reduce modeling time by approximately 95

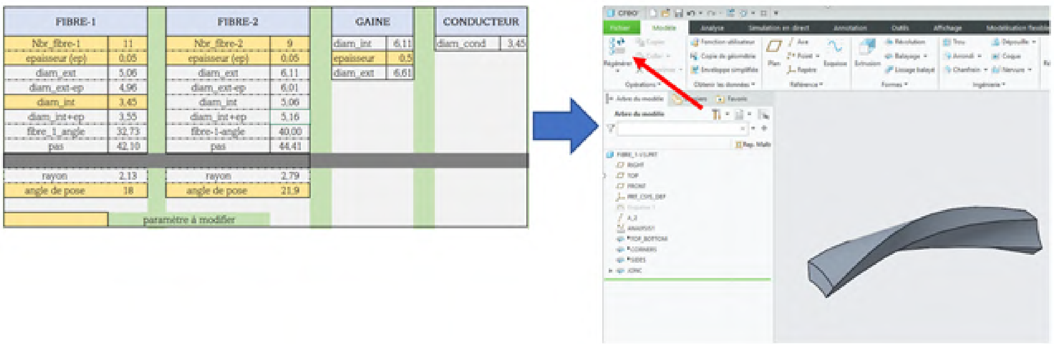

Figure 2.2: CAO model in Creo.

2.3 creation of the simulation model

2.3.1 Meshing

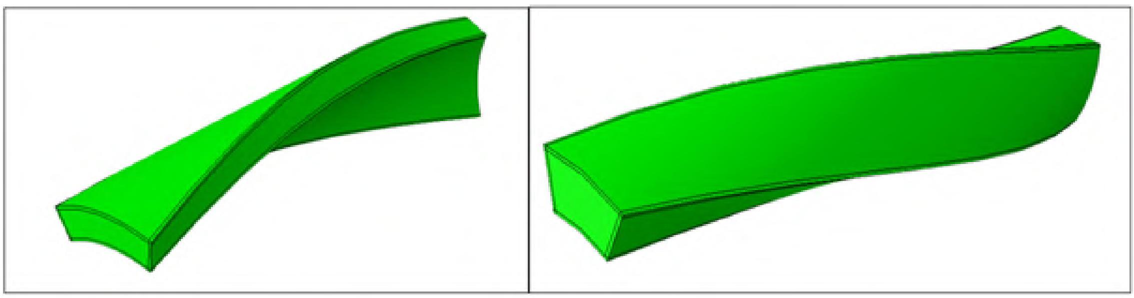

Figure 2.3: Creo parts that allow us to have an adjusted mesh.

Creo directly generates the cable part that are suitable to make a mesh of set elements and allows us to perform a hexahedral element mesh knowing that this type of meshing is crucial to the convergence of the simulation results.

It was observed by ***Cetim*** that full integration of hybrid parts made convergence simpler. The elements are in fact heavily loaded with complicated stresses, particularly in the bi-compression S22-S33 region. Then, entire formulation should be used.

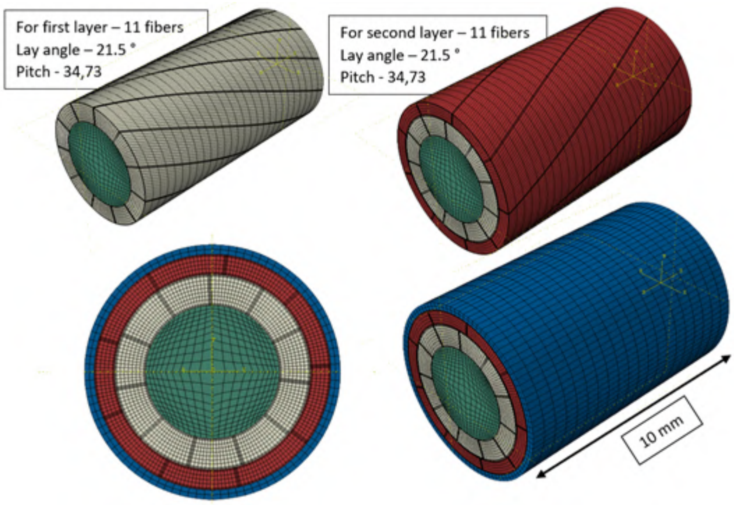

Figure 2.4: Meshing on Abaqus.

As a reminder that a length of 10 mm was modeled in order to reduce the time of calculations, so this length contains approximately 65 439 elements in function of the simulated parts.

2.3.2 Material orientation setup

The global reference frame's z-axis is aligned with the cable primary direction. Each of the components, especially the strands, has its unique material orientation in relation to its constitution or simply to make it easier to analyze the behaviors in local reference frames:

- The strand's local orientation is changing in accordance with its helix, with direction 1 corresponding to the direction of the fibers.
- In a manner like that of the strand, the conductor and outer sheath are also orientated, with direction 1 being along the global z, direction 2 being along the circumference, and direction 3 being along the thickness

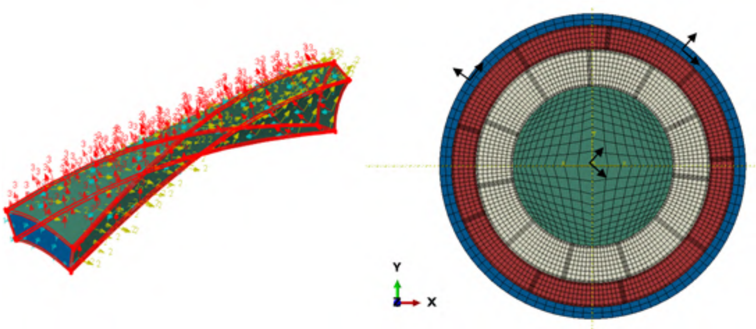

Figure 2.5: Cable spatial orientation covention and local material index.

2.3.3 Boundary conditions and loading

The traction on the cable is the load considered for the reference scenario. It is assumed that the rope is initially stress-free. Remember that after winding, the strands are cured.

To do this, an axial displacement is delivered to each node on one of the modelled cable ends. Therefore, the displacement of 0.25 mm is used for a modelled length of 10 mm, resulting in a 2.5 percent deformation range.

Regarding the boundary conditions, the opposite end of the cable is blocked both axially and rotationally in accordance with a cylindrical reference. In order to stabilize the assembly and enable the convergence of the calculation, the sections of the sheath and conductor located in the XY and YZ planes are likewise blocked-in rotation. In fact, the entire wire will inflate in an unphysical way if the part is not blocked-in rotation. Nevertheless, the results of the many experiments conducted indicate that it has little impact on how the cable behaves and the analysis that follows.

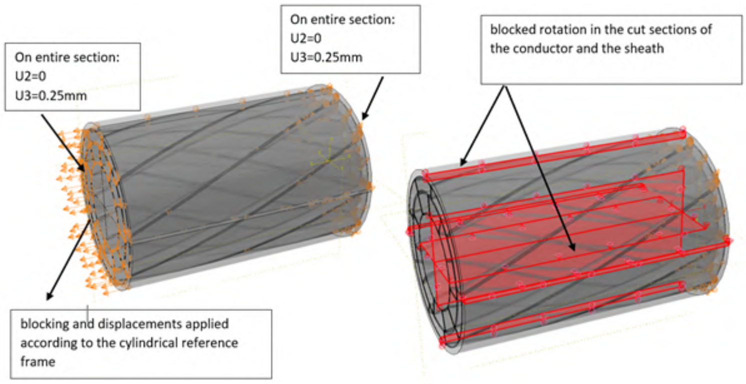

Figure 2.6: Case of traction: Imposed displacement.

2.3.4 Interactions and constraints

Contact setup

- ***Radical contact***

It has been assumed that the composite part's rod is properly attached to the coating that surrounds it, which is 0.05 mm thick. However, the contact is controlled by the several strands (jonc + coating around). This interaction may take the form of complete bonding or touch.

Consideration has been given to the pair/finite, sliding/surface-to-surface, contact option, where each contact between opposing surfaces is determined.

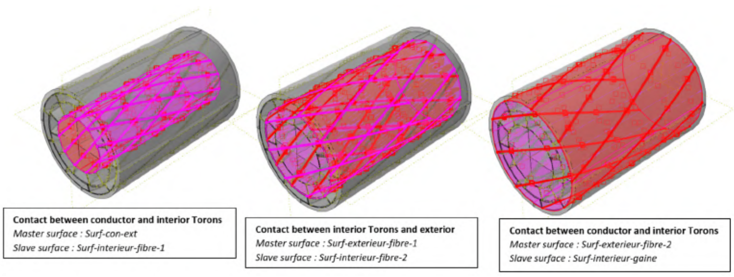

Figure 2.7: Radical contact.

A master surface and a slave surface must be specified for the pair type contact. Every contact surface is either a master or a slave, not both. It was then essential to restrict the contact surface in the case of strands that are in contact on both sides by deleting the corner element so there are no nodes shared by the master and slave surfaces.

- ***Side contact***

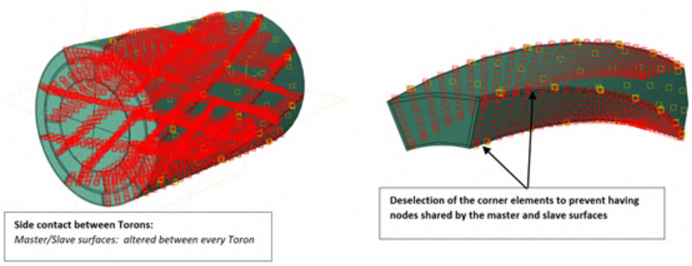

Figure 2.8: Side contact.

The contact is deemed to be without friction to allow the parts to slide freely in relation to each other in order to restrict the potential interactions between the many components that make up the cable.

Numerical sticking (Tie)

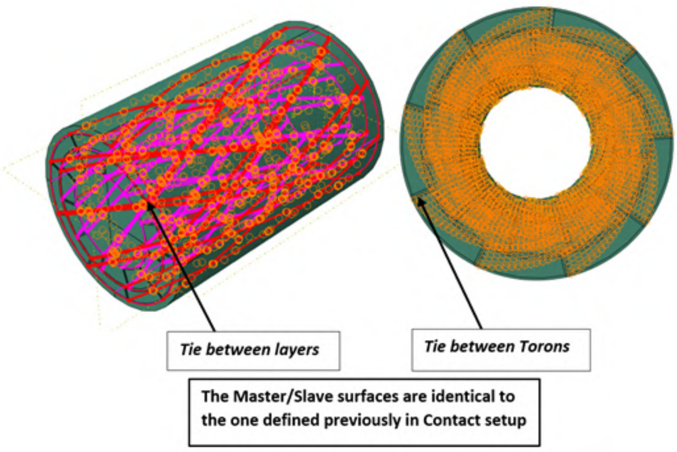

Figure 2.9: Numerical sticking (Tie).

we apply a tie between all these parts to consider that they are perfectly stuck to each other, which is mainly what describes the behavior of our cable in real life.

2.4 Conclusion

The calculations are performed in geometric nonlinear statics with linear elastic material properties, which according to the data above being the closest characteristics that better describe the cable behavior.

Chapter 3

Simulation results

3.1 Introduction

We were able to conduct a lot of simulations while varying the lay angles of the two layers of the cable and the number of fibers in each layer by following the instructions in chapter 2.a sample of the configuration that we were interested in was selected and the simulation's results along with the resulting conclusions will be provided in this chapter.

3.2 Results visualization

3.2.1 Configuration 1

	Number of fibers	Lay angle (°)	Pitch (mm)
Interior layer	11	21.5	34.73
Exterior layer	9	19.5	50.40

Table 3.1: First configuration's characteristics.

Displacement results

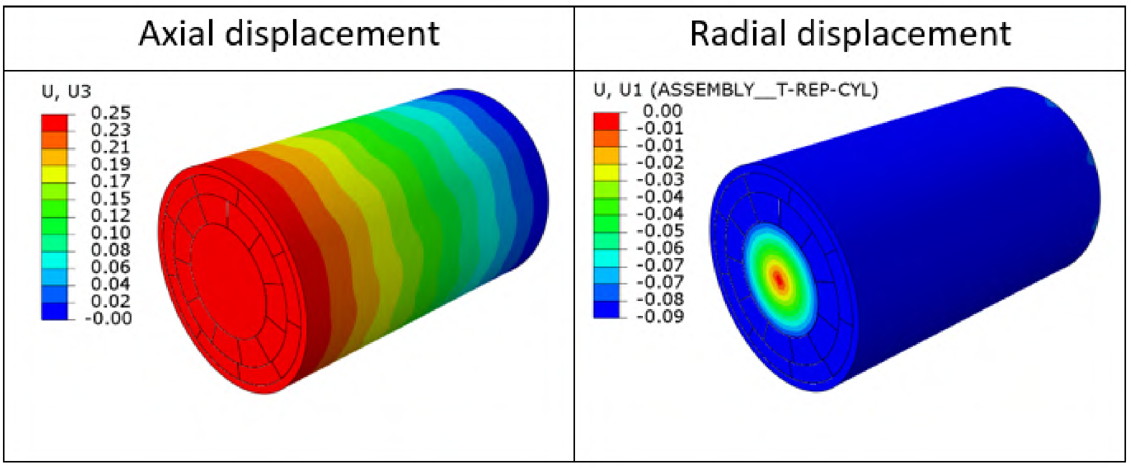

Figure 3.1: Displacement visualization at 2.5%.

the axial displacement because of the action of Poisson's ratio. Recall that in order to visualize the event, the ends had to be blocked in rotation. In the case of bonding between all parts, the entire cable shrinks by a maximum of 0.09 mm at the radius.

Visualization of contact pressures

The contact pressure was calculated at the Safe Working Load which is a value determined at approximately the half of the Breaking Load of the cable, In the case of our cable it is determined at 3000 lbs (which is equivalent to 13.344 KN).

Based on the result it was confirmed the detachment of the sheath from the strands while applying traction force.

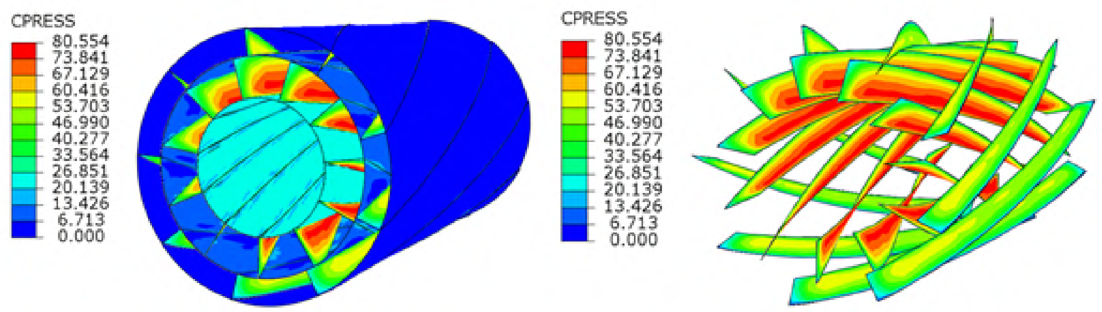

Figure 3.2: Contact pressure at Safe Working Load (SWL).

The contact pressure is zero at the radial contact with the outer sheath and reaches its maximum value of 80.554 MPa at the tangential contact between the strands of the first (inner) layer.

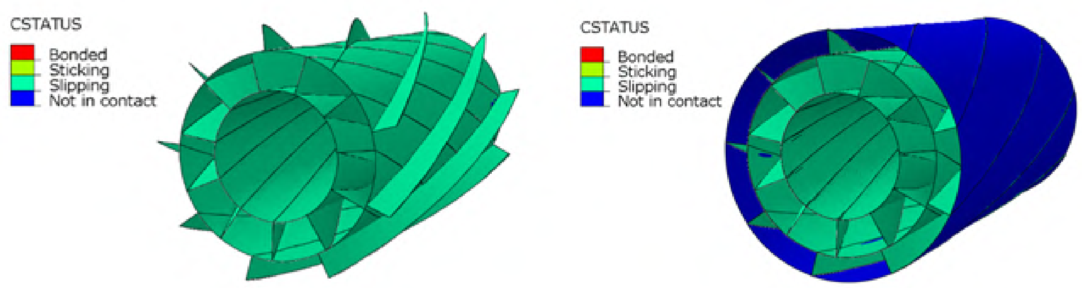

Figure 3.3: Contact STATUS.

The jacket loses contact with the strands of the second crown because the radial shrinking of the strands is larger than that of the jacket (blue part).

Stiffness results

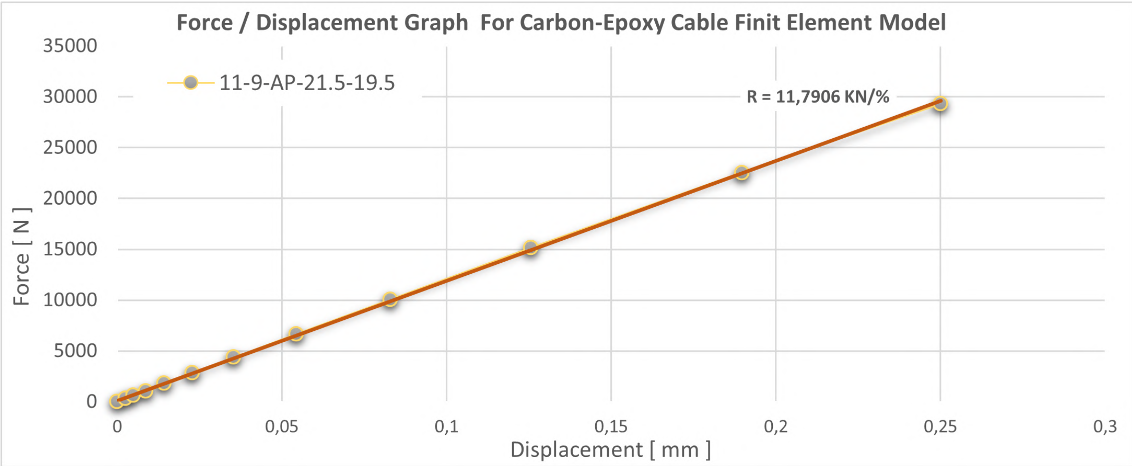

Figure 3.4: Rigidity for 11/9 configuration at 2.5 %.

For the situation with Tie, we obtain a fairly linear response and a stiffness of 11.7 KN/%; the variance of the stiffness is primarily influenced by the number of strands.

Constraints results

The visualizations of the various stress components in the median section of the modelled joncs are displayed in the tables below. The figures shown are average values determined across the entire length of a jonc while accounting for its tiny size and the many numerical details presented.

Note: Because the mesh size is consistent, the average stress is determined by averaging over all of the section's components.

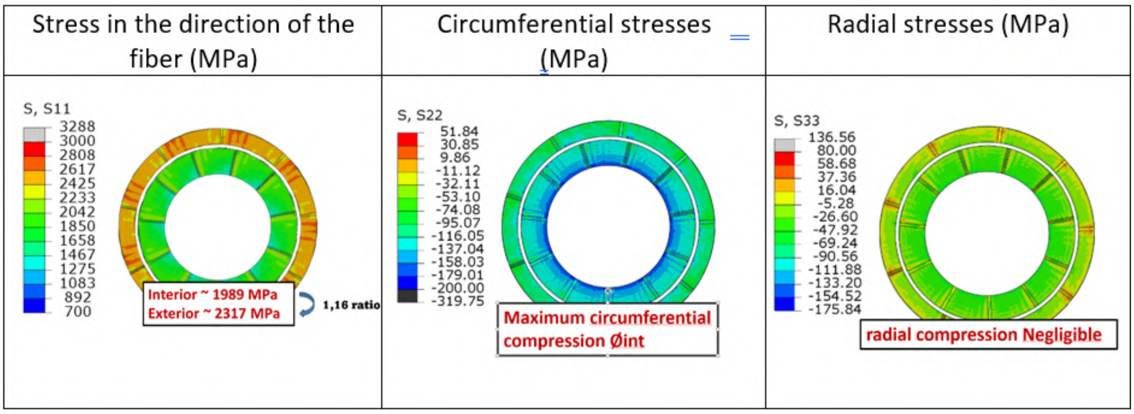

Figure 3.5: Directional stresses (MPa) in the middle section of the jonc at 2.5% strain.

The stresses in the direction of the fiber under the influence of traction indicate that the outer crown of the jonc is where they are most stressed, which is compatible with the angle of the joncs and their proportions.

In actuality, the outer jonc's laying angle (19.5°) is less than the inner one (21.5°). Because they are more aligned and numerous, they have an equivalent stiffness in the direction of the rope that is more significant and absorbs more of the tensile force. We achieve an average of 2317 MPa in the outer rings, whether in contact or in tie, and this decreases to 1989 MPa in the inner ring, which is a ratio of 1,1.

We find stress values at % strain that are relatively close to the theoretical breaking point, which is thought to be 2842 MPa in the fiber direction.

It is observed that all the joncs are compressed circumferentially, with greatest values on the inner diameter side. The joncs are also compressed in a radial way. The crack propagation caused by the shear is constrained by this bicompression.

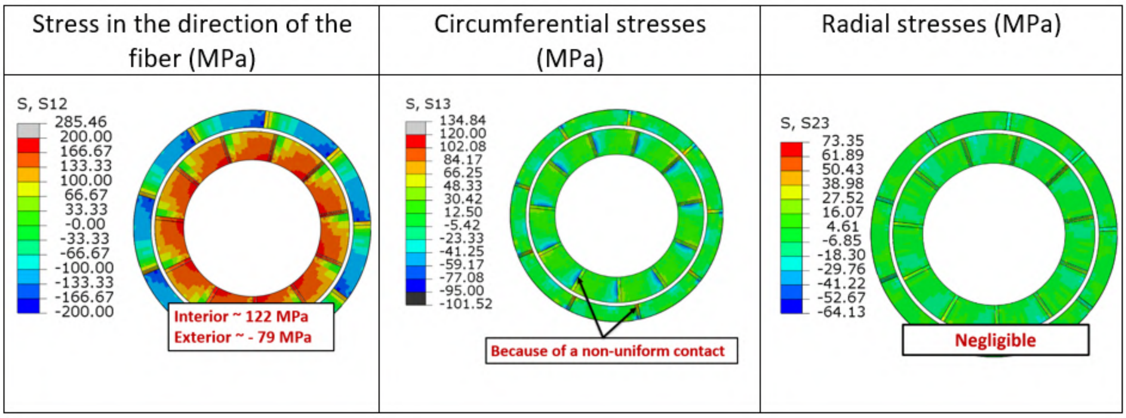

Figure 3.6: Shear stresses (MPa) in the middle section of the jonc at 2.5% deformation.

The inner strands of the S12 plane sustain shear stresses on average of 122 MPa at 2.5 percent strain. The common theoretical failure limits adopted are typically low (30 to 90 MPa). Compared to digital bonding, the S12 shear for contact management is more evenly distributed across the inner and outer joncs.

The two main factors contributing to the failure of the rope are the stress in plane shear and the tension in the fiber direction. With all the caveats on the model's level of fidelity, we were able to estimate the value of the torque (S11, S12) that causes the rupture by correlating the tests with the model (Cf. curves below).

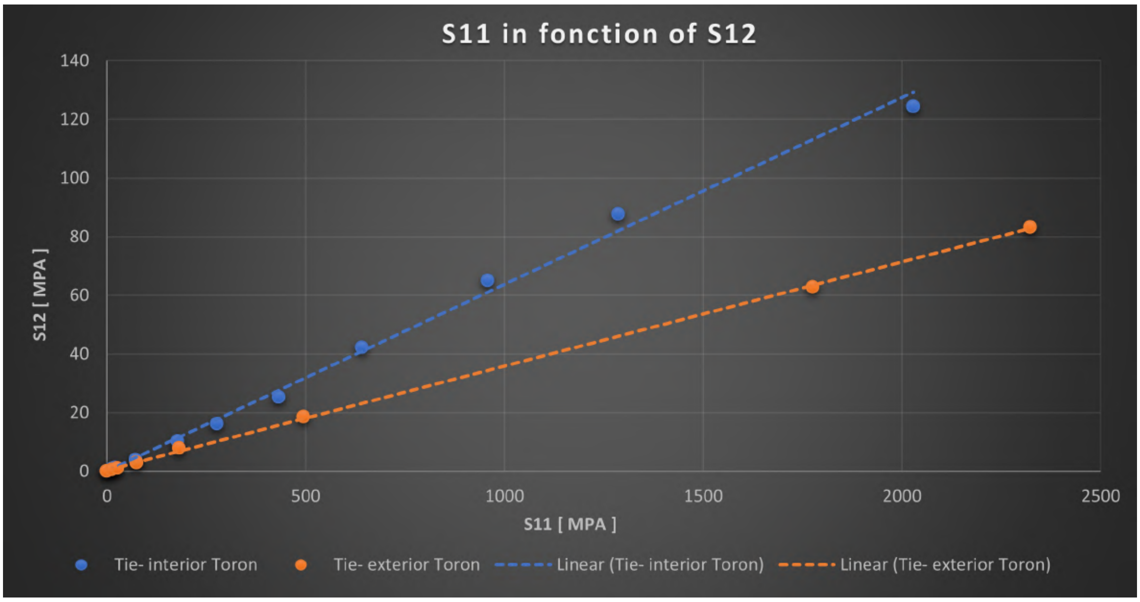

Figure 3.7: Rupture envelope.

Out-of-plane shear stresses are basically nonexistent throughout. Local stresses on the edges are seen for the shear involving tangential contact between the strands (S13), which are likely connected to the necessity of excluding components of the strands' edge from the selections for the case with contact or with tie.

In the scenario when the parts are assumed to be coupled together, the coupling behavior between S11 and S12 is slightly linear (tie).

The rupture envelope is essential for the validation of the numerical model, as we can determine the point where our cable is more suited to be broken.

3.2.2 Configuration 2: Optimized

	Number of fibers	Lay angle (°)	Pitch (mm)
Interior layer	11	18	42.10
Exterior layer	9	21.9	44.41

Table 3.2: Second configuration's characteristics.

the choice of this configuration was based on the fact that it was already proceeded in the manufacturing of the experimental prototype ENP3, and that will be used later for validation purposes.

Displacement results

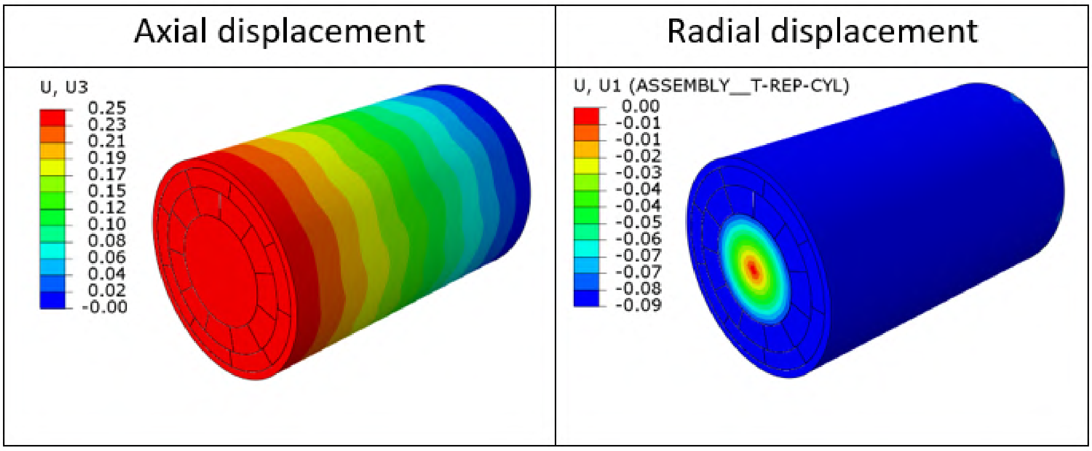

Figure 3.8: Displacement visualisation at 2.5 %.

Stiffness results

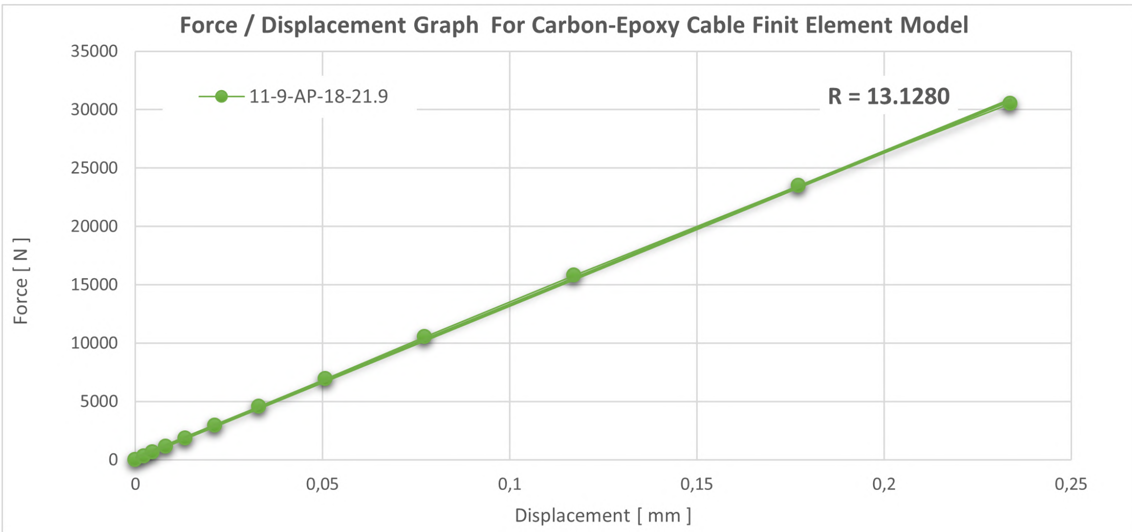

Figure 3.9: Rigidity for 11/9 configuration at 2.5 %.

The stiffness results for the optimized configuration of a lay angle of 18-21.9 has a rigidity value of 13.1 KN/%.

Constraints results

The visualizations of the various stress components in the median section of the modelled joncs are displayed in the tables below.

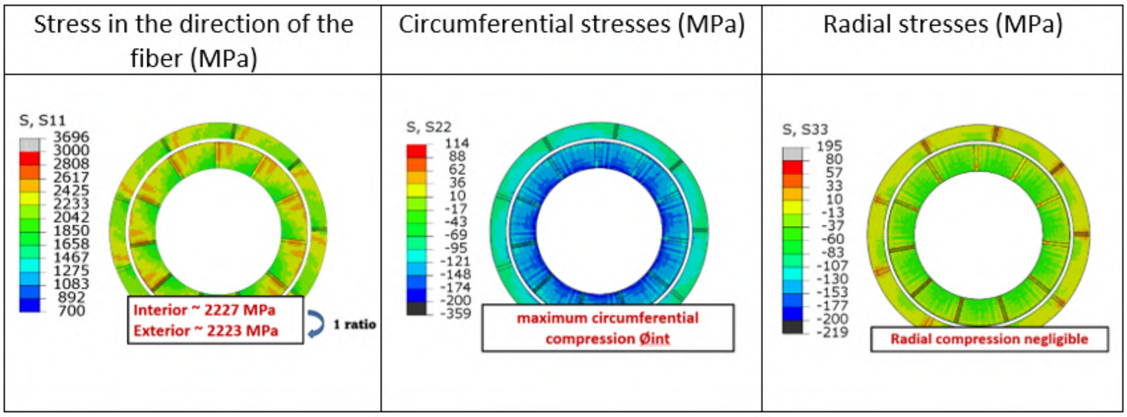

Figure 3.10: Directional stresses (MPa) in the middle section of the jonc at 2.5% strain.

The stresses in the direction of the fiber under the influence of traction indicate that inner and outer crows have approximately the same value of stress, which is compatible with the angle of the joncs and their proportions. In actuality, the outer jonc's laying angle (21.9°) is bigger than the inner one (18°). Based on the number of the Torons in every layer, our new configuration can absorb more tensile for due to the gain of rigidity.

We achieve an average of 2223 MPa in the outer rings, along with a value of 2227 in the inner crown which gives us a ratio of 1. We can safely say that this configuration of lay angles has made us more stable in terms of stress between first and second layer.

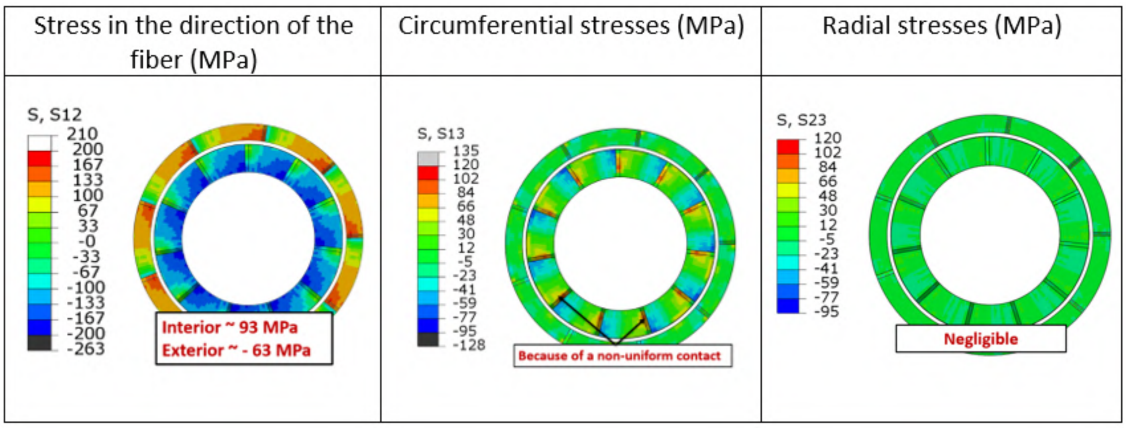

Figure 3.11: Shear stresses (MPa) in the middle section of the jonc at 2.5% deformation.

The inner strands of the S12 plane sustain shear stresses on average of 93 MPa while the outer joncs have shear stresses valued at 63 MPa at 2.5 % strain.

The circumferential stresses and the Radial stresses are practically negligible. We proceed to creating the rupture envelope in function with S11 and S12 that intervene mainly in the rupture of the cable.

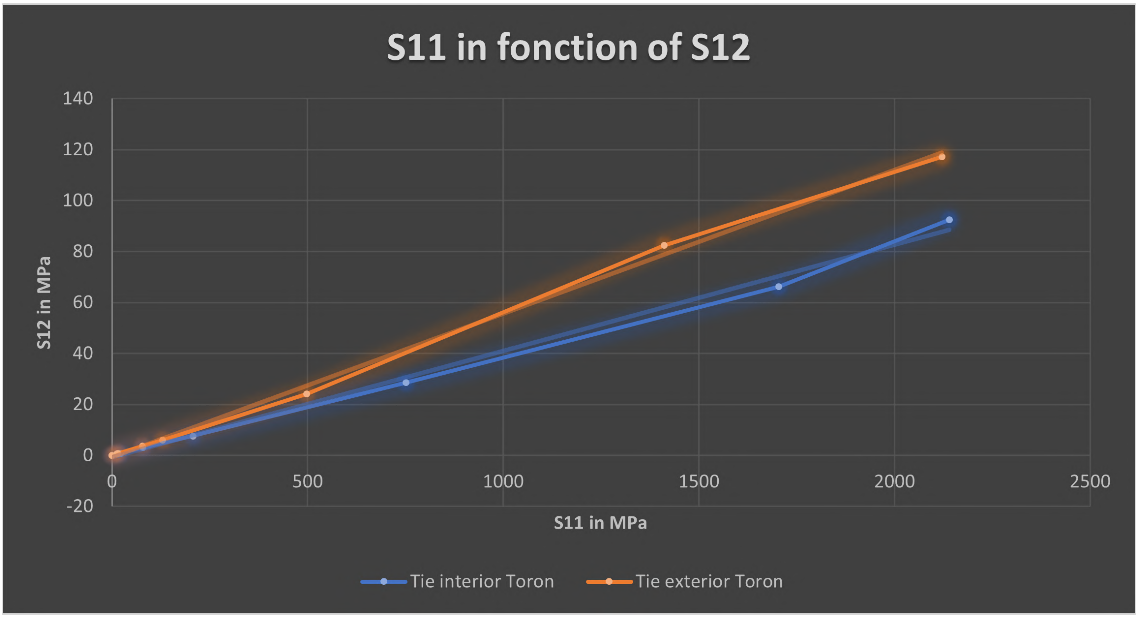

Figure 3.12: Rupture envelope.

3.2.3 Comparison of our current configuration and our optimized one

Torque results

Configuration	Pitch Angle		Fiber-Torque [N.mm]		Cable-Torque [N.mm]
	FIBRE-1	FIBRE-2	FIBRE-1	FIBRE-2	
11/9	21.5	19.5	11 877	-14 388	- 2 511
	18	21.9	12 038	-14 416	- 2 378

Table 3.3: Torque values (N.mm) in function of Pitch angles for an axial force of 32.3 kN.

Optimizing the numerical model of the previous configuration with pitch angles of 21.5 in the first layer and 19.5 in the second allowed us to gain about 6% stability by changing the pitch angles to 18 in the first layer and 21.9 in the second. we were able to reduce the torque generated in the cable from 2511 N.mm to 2378 N.mm. and by performing more simulations, we were able to reduce the torque generated up to 1714 N.mm, resulting in a 31% more stable cable.

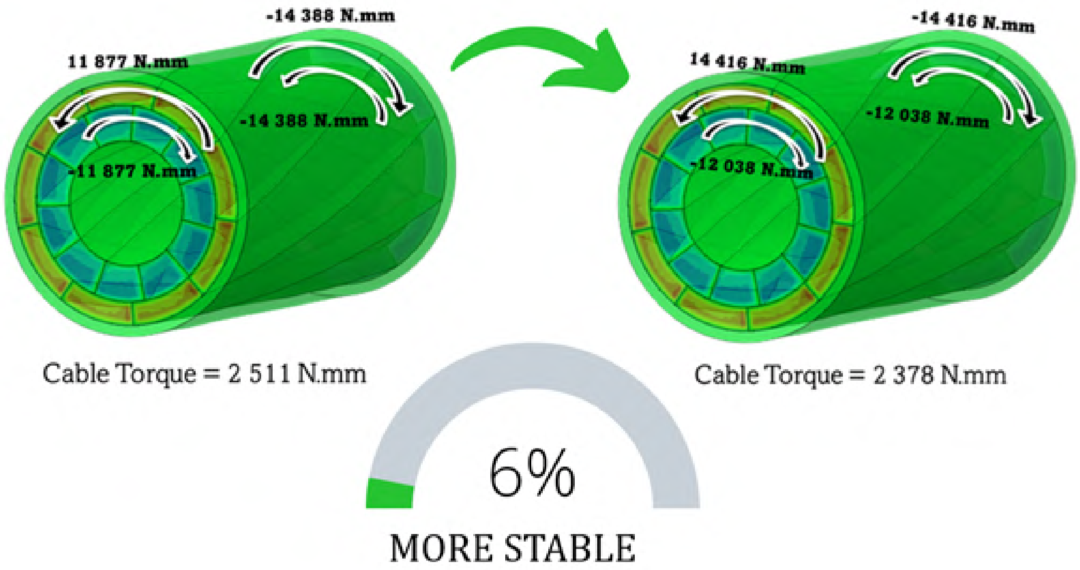

Figure 3.13: Visualizations of the different torque components generated in the modeled joncs.

Constraint in the direction of the cable

Pitch Angle		S11 - average Stress [MPa]		S11 - Minimal Stress [MPa]		S11 - Maximum Stress [MPa]	
FIBRE-1	FIBRE-2	FIBRE-1	FIBRE-2	FIBRE-1	FIBRE-1	FIBRE-1	FIBRE-2
21.5	19.5	1989	2317	1395	1834	2455	2631
18	29.5	2227	2223	1611	1765	2615	2535

Table 3.4: Stress values in the fiber direction S11 (MPa) in the middle section of the joncs for an axial force of 30.5 kN.

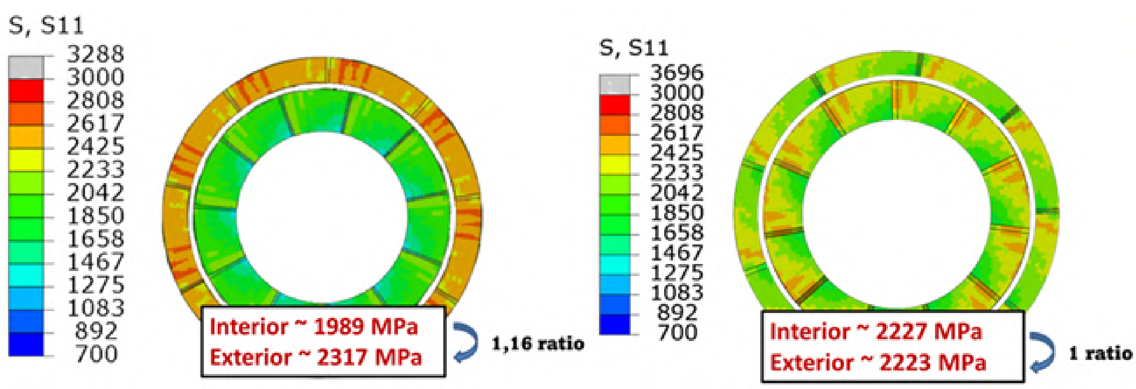

Figure 3.14: Visualizations of the different torque components generated in the modeled joncs.

In terms of stresses along the cable, changing the angles of inclination will allow us to get a more balanced cable as shown above, we were able to get a value of 2227 MPa in the inner crown and a value of 2223 MPa in the outer crown, which gives us a ratio of 1 compared to a ratio of 1.16 in the old configuration.

Shear stress

Pitch Angle		S12 - Average stress [MPa]		S12 - Minimum Stress [MPa]		S12 - Maximum Stress [MPa]	
FIBRE-1	FIBRE-2	FIBRE-1	FIBRE-2	FIBRE-1	FIBRE-2	FIBRE-1	FIBRE-2
21.5	19.5	122	-79	-10	-175	190	107
18	29.5	93	-63	-24	-110	164	-135

Table 3.5: Values of shear stresses S12 (MPa) in the middle section of the rushes for an axial force of about 30.5 kN.

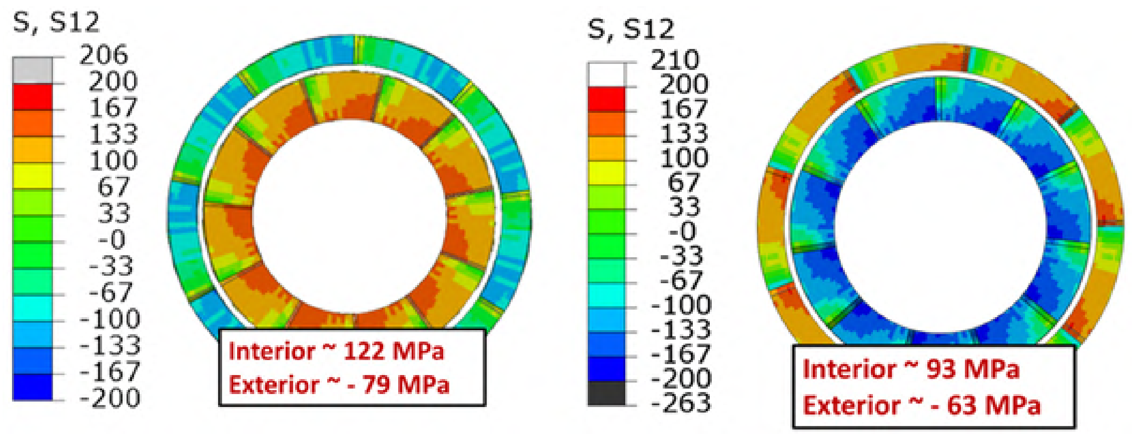

Figure 3.15: Visualizations of the different components of stresses S12 in the middle section of the modelled joncs at 30.5 KN.

The shear stresses in the S12 plane are moderate by an average of 73 MPa which is within the theoretical fracture limits usually taken (30 to 90 MPa) knowing that these values are generally taken low.

Stifness

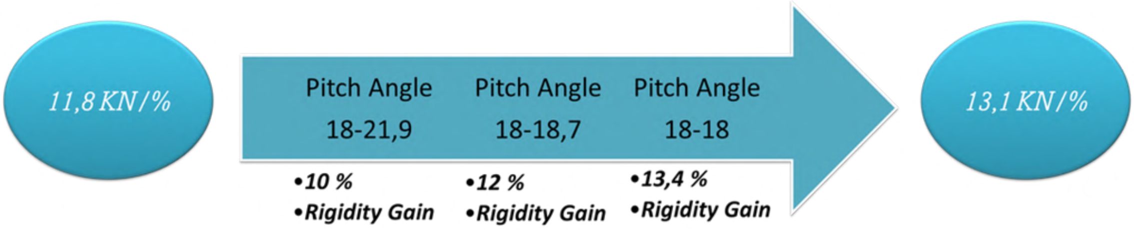

Figure 3.16: Rigidity gain while changing the lay angles for 11/9 configuration.

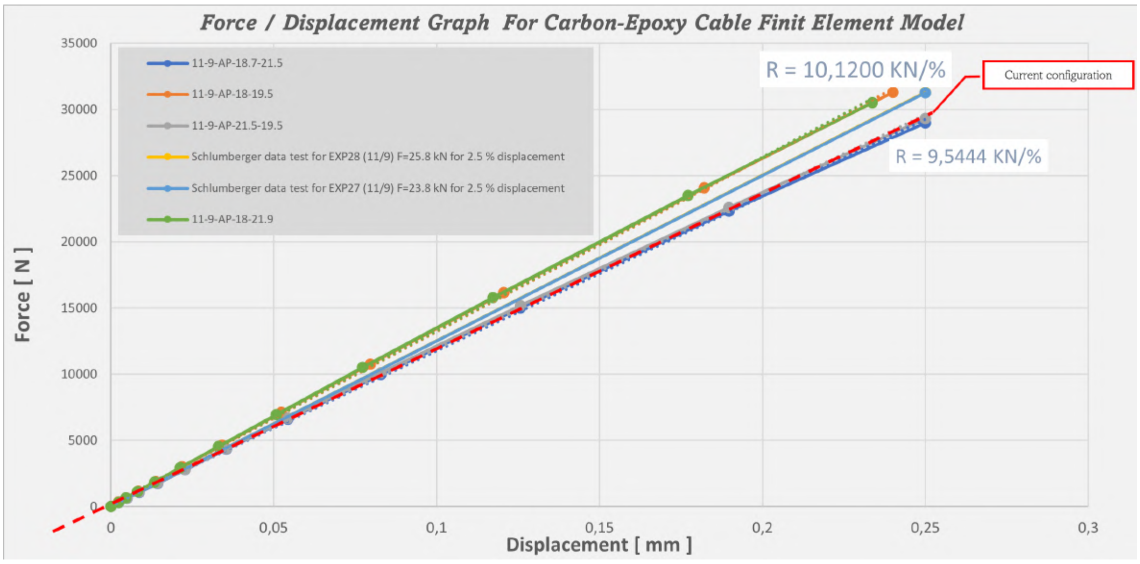

Figure 3.17: validation of the FE model with EXP27/EXP28 cable prototypes.

For both cases, we obtain a linear behavior for both configurations, the rigidity for the new configuration is greater than that of the old configuration. We therefore obtain a stiffness value of about 13.1 KN/% in the new configuration compared to 11.8 KN/% in the old one, which gives us a stiffness gain of about 10%.

3.3 Conclusion

Chapter 4

StreamLINE Cable

4.1 Introduction

In intervention, workover, and completion operations across all environments, StreamLINE polymer-locked wireline cable efficiently overcomes the issues caused by the usage of traditional wireline cable. Maintenance visits caused by grease injection, armor stranding, bird caging, corrosion, and twisting are all but nonexistent. The end result is a considerable increase in efficiency with decreased operational and well control hazards, as well as logistics- and cost-related maintenance.

To ensure total immunity against well fluids like gas entering the cable, StreamLINE cable is torque balanced and offered as a system with an integrated dual pack off and specially constructed sealed torpedo.

The interest in the streamLINE was based on the fact that is the direct competitive to our composite cable, so a benchmarking is considered a good idea to know where we are in comparison to the streamLINE cable that is considered a state-of-the-art model in wirelines world.

4.2 General description

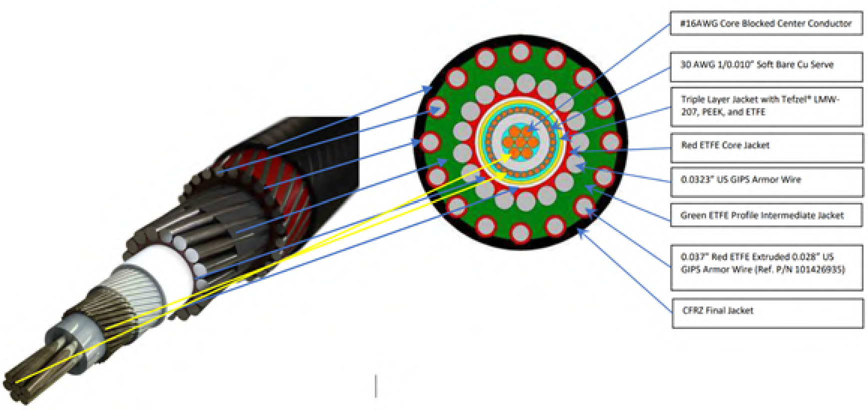

Figure 4.1: The cable composition.

A 16 AWG core blocked conductor with Tefzel, PFA insulation makes up the cable core. Insulation is placed on top of a further Tefzel layer, which acts as a serving bed. The conductors used in it are AWG conductors. A red ETFE core jacket is placed on top of a triple layer jacket made of Tefzel, PEEK, and ETFE. The core jacket has the first pass armor wires incorporated into it, and the next layer is a profiled intermediate jacket made of green ETFE. The second pass armor is made up of coated-solid armor wires that are inserted into the intermediate jacket. The final CFRZ jacket completes the cable.

4.3 Designing and modeling of the StreamLINE cable

Under ***Creo***, the creation of a total 6 parts will be made to complete the assembly of the cable under ***Abaqus***.

4.3.1 Coating

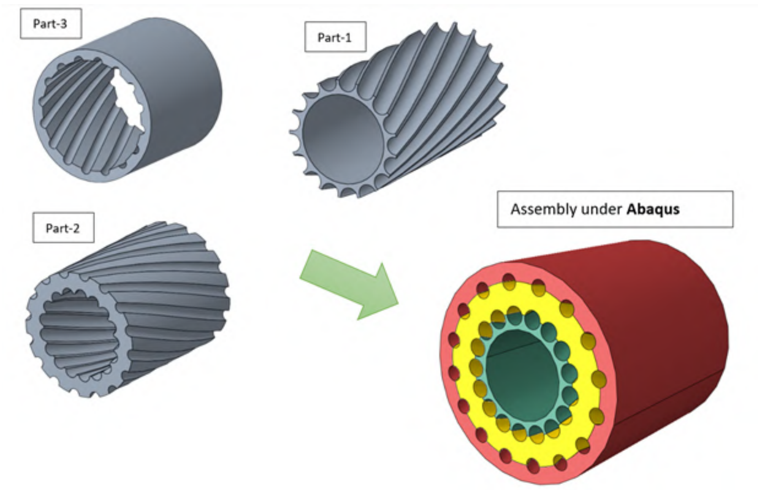

Figure 4.2: Coating.

4.3.2 First and second layer of armoring

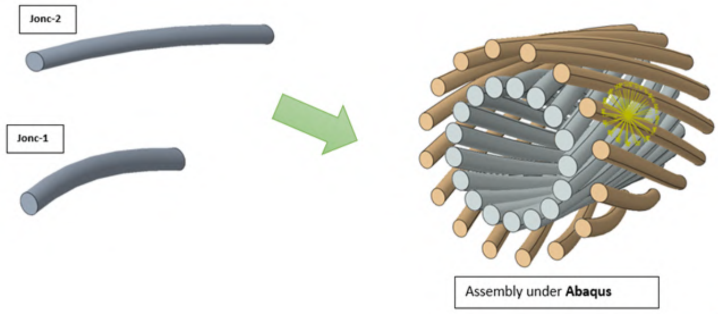

Figure 4.3: First and second layer of armoring.

4.3.3 Conductor

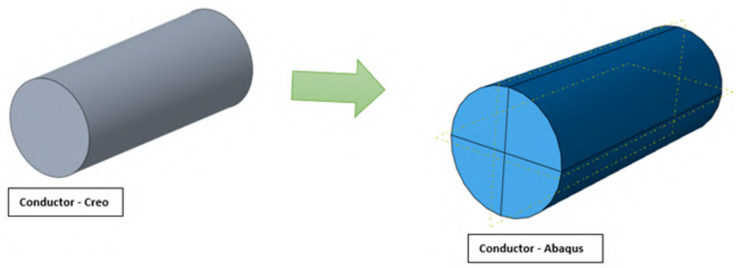

Figure 4.4: Conductor.

4.3.4 Final assembly

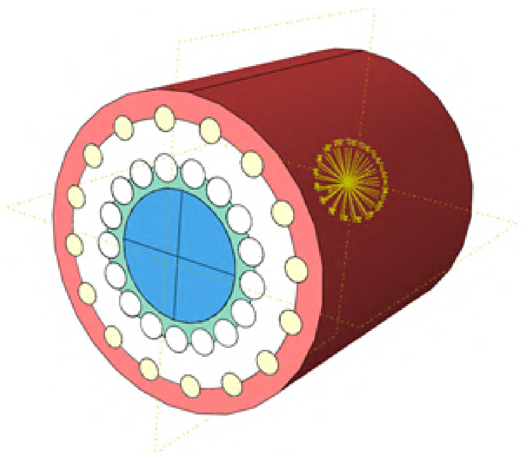

Figure 4.5: Final assembly.

4.4 Creation of the simulation model

4.4.1 Meshing

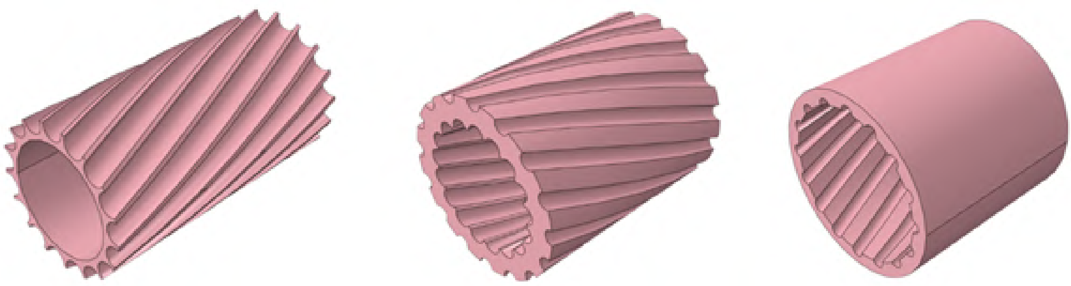

Figure 4.6: Free structure meshing.

Because of the complex structure of the coating, a free meshing will be in order, using a tetrahedral meshing with hybrid element.

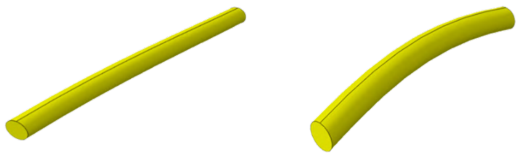

Figure 4.7: Sweep meshing for the joncs.

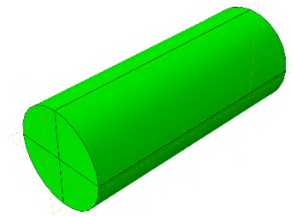

Figure 4.8: Structured meshing for the conductor.

For the steel joncs and the conductor, a hexahedral meshing will be in order for our streamLINE model.

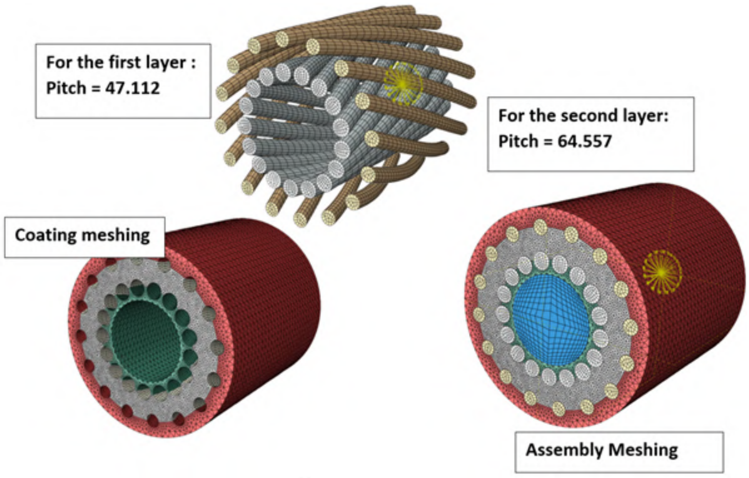

Figure 4.9: Cable meshing.

As a reminder that a length of 10 mm was modeled in order to reduce the time of calculations, so this length contains approximately 282 386 elements in function of the simulated parts.

4.4.2 Material orientation setup

The z-axis of the global reference frame coincides with the principal direction of the wire. To make it simpler to examine the behaviors in local reference frames, each of the components, notably the strands, has a distinct material orientation in regard to its constitution:

- The strand's local orientation is changing in accordance with its helix, with direction 3 corresponding to the direction of the fibers.
- In a manner like that of the strand, the conductor and outer sheath are also orientated, with direction 3 being along the global z, direction 2 being along the circumference, and direction being along the thickness

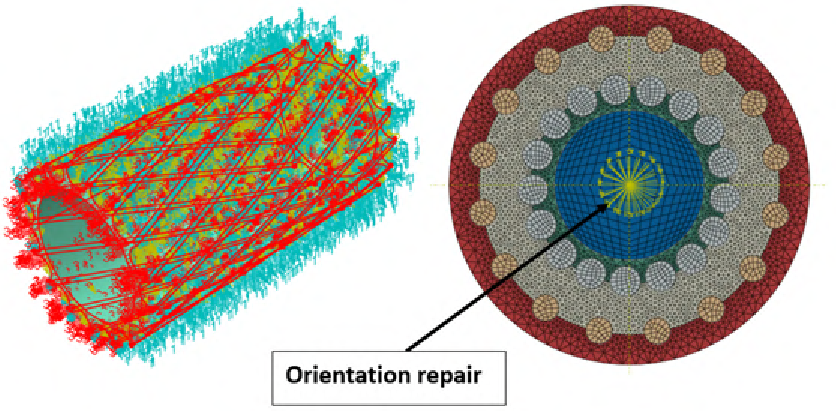

Figure 4.10: Cable spatial orientation convention and local material index.

4.4.3 Boundary conditions and loading

The load taken into account for the reference case is the traction on the cable. The rope is said to be initially stress-free. Keep in mind that the strands are cured after winding. To do this, each node on one of the simulated cable ends receives an axial displacement. As a consequence, a displacement of 0.25 mm is employed for a model length of 10 mm, producing a deformation range of 2.5 percent.

Regarding the boundary conditions, a cylindrical reference is used to block the cable's opposite end both axially and rotationally. The parts of the sheath and conductor situated in the XY and YZ planes are also blocked-in rotation, which stabilizes the assembly and enables computation convergence. In reality, if the portion is not blocked in rotation, the entire wire will swell in an illogical manner. However, the results of the numerous studies show that it doesn't significantly affect how the cable acts or the analysis that follows.

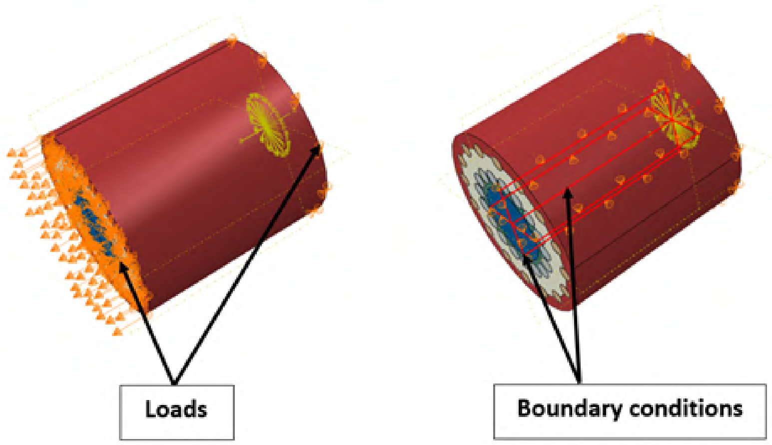

Figure 4.11: case of traction: imposed displacement.

4.4.4 Interactions and constraints

Contact setup

- Radial contact

The different parts of the coating have been assumed glued one another to better describe the cable behavior while experiencing a tensile force.

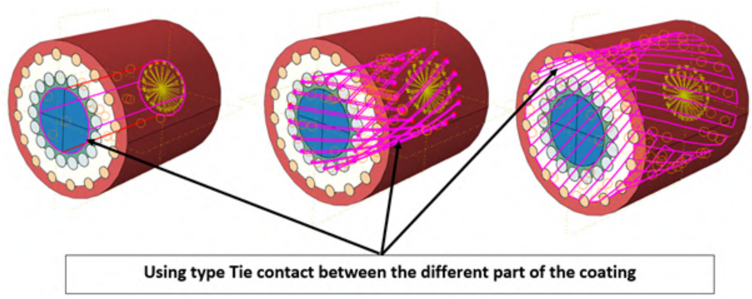

Figure 4.12: Radial contact.

- Side contact

The contact is deemed to be without friction to allow the parts to slide freely in relation to each other in order to restrict the potential interactions between the many components that make up the cable.

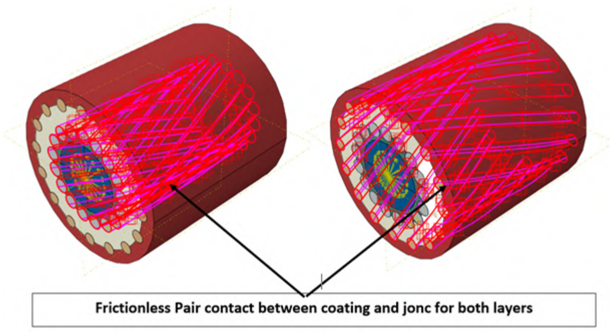

Figure 4.13: Side contact.

4.5 Simulation results and model validation

4.5.1 Visuakization of contact pressures

The contact pressure was computed at the cable's Safe Working Load, which was established at a value equal to about half of the cable's Breaking Load in the case of our cable (5000 lbs for the StreamLINE cable). which measures as 22.2 KN.

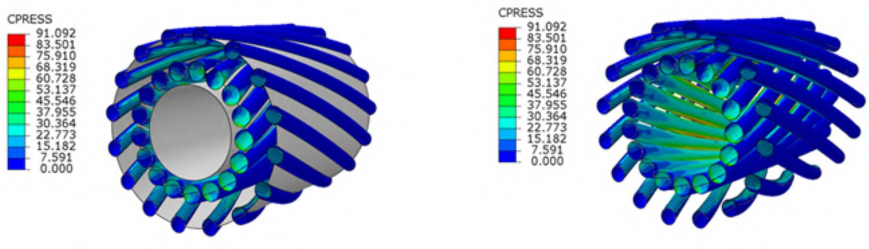

Figure 4.14: Contact pressure (MPa) - For Safe Working Load - 1.1%.

At the radial contact with the outer sheath, the contact pressure is zero, and at the tangential contact between the strands of the first (inner) layer, it reaches its maximum value of 91.092 MPa.

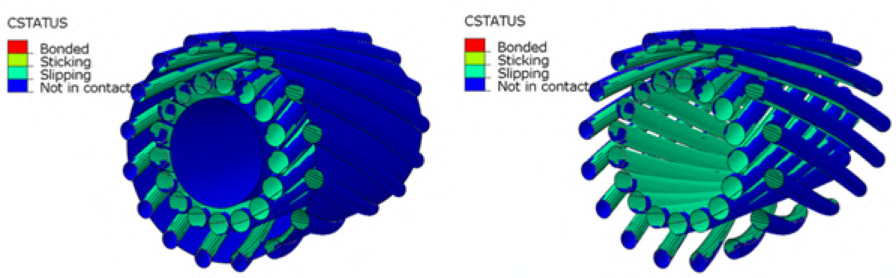

Figure 4.15: Contact STATUS.

The sheath loses also contact with the strands of the second crown because the radial shrinking of the strands is larger than that of the sheath (blue part).

4.5.2 Stifness results

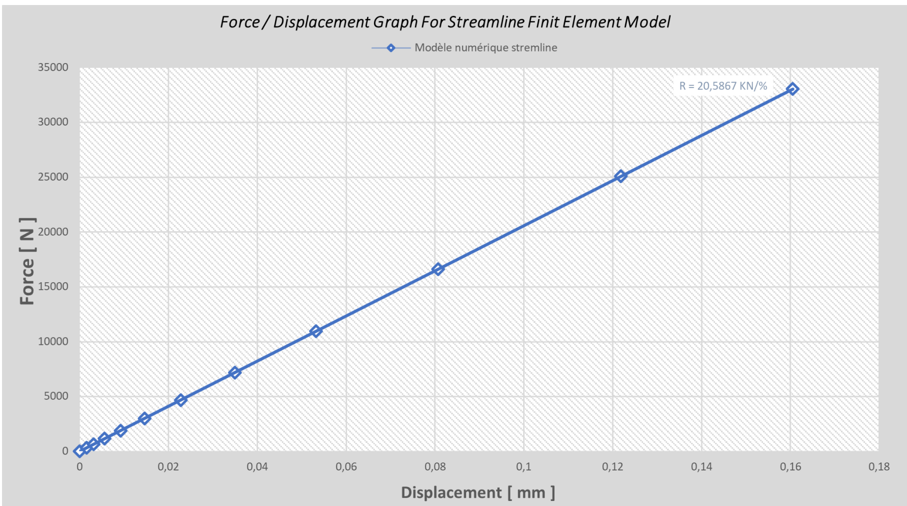

Figure 4.16: Stiffness results.

For the situation with Tie and frictionless contact, we obtain a fairly linear response and a stiffness of 20.5 kN/%, the variance of the stiffness is primarily influenced by the number of strands.

4.5.3 Constraints results

The visualizations of the various stress components in the median section of the modelled joncs are displayed in the tables below. The figures shown are average values determined across the entire length of a jonc while accounting for its tiny size and the many numerical details presented.

Note: Because the mesh size is consistent, the average stress is determined by averaging over all of the section's components.

Stress in the direction of the fiber (MPa)	circumferential stresses (MPa)	Radial stresses (MPa)
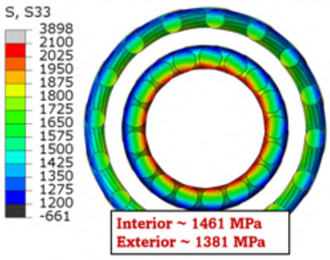	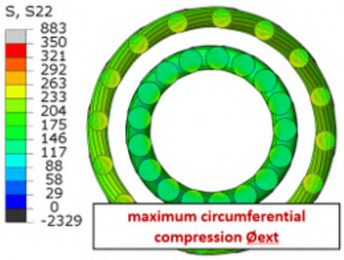	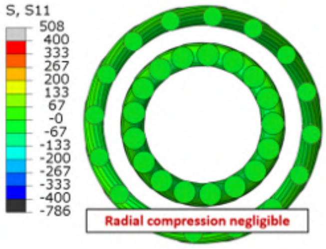

Figure 4.17: Stiffness results.

The outer crown of the jonc is where they are most strained, according to the stresses in the direction of the fiber under the impact of traction, which is consistent with the angle of the joncs and their proportions. Actually, the pitch of the outer jonc is 64.557, whereas the pitch of the inner jonc is 47.112. They have an analogous stiffness in the direction of the rope that is more substantial and absorbs more of the tensile force because they are more aligned and numerous. Whether in touch or in a tie, we reach an average of 1381 MPa in the outer rings, and this go up to 1461 MPa in the inner ring, or a ratio of 1,05.

4.5.4 Model validation

Based of the test results conducted on the StreamLINE cable we were able to validate our model with a minimum margin of error. Considering the stiffness, below are the results: The test results showed a rigidity of approximately 19.86 KN/% while the finite element model gave a result of 20.5 KN/%. The slight difference of the results could be explained with numerous reasons.

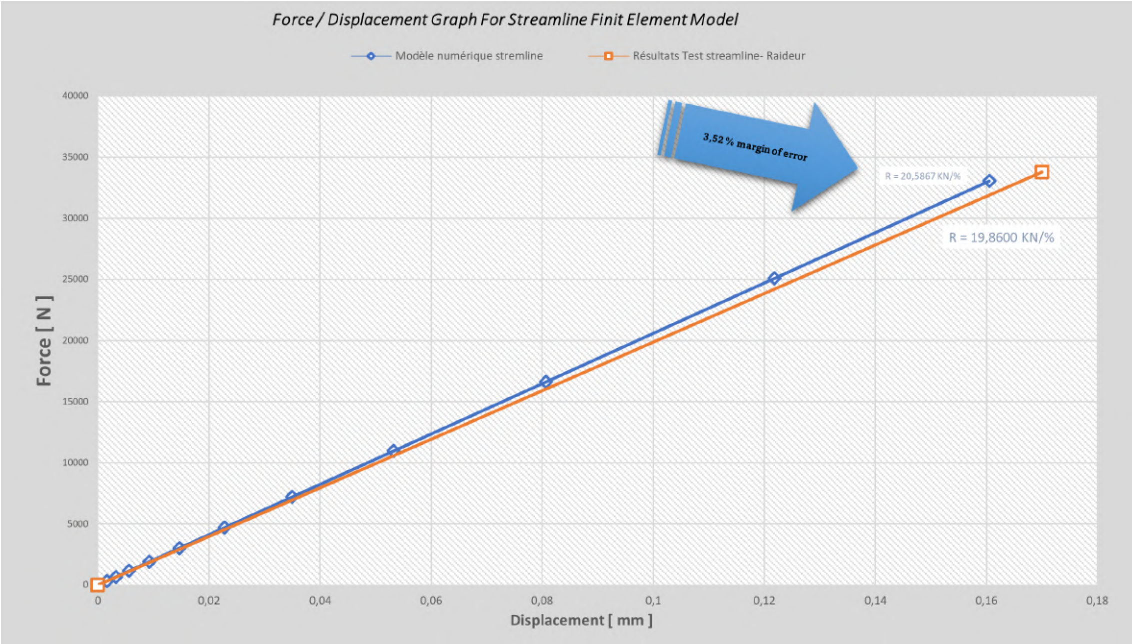

Figure 4.18: Difference between StreaLINE model and the test results.

In terms of Torque, the graph bellow shows the torque results experimentally and the results given by our model.

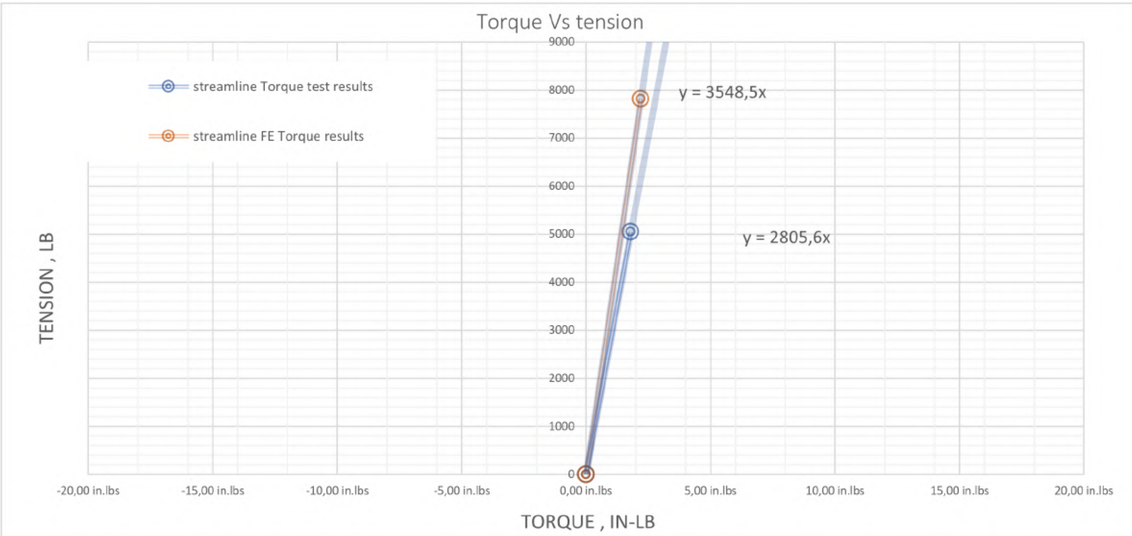

Figure 4.19: Torque results (test and finite element model).

4.6 Conclusion

Our ***StreamLINE*** is validated and will be used in future steps to determine where we are in our development and optimization of the cable, a benchmarking step will be in order after the validation of the carbon/epoxy model with a well-chosen samples and prototypes will be made to check our calculations.